Matrix Biology 145 (2026) 19–31

Contents lists available at ScienceDirect

Matrix Biology

journal homepage: www.elsevier.com/locate/matbio

# Abnormal extracellular matrix deposition by fascial fibroblasts underlies the connective tissue pathology in the disease Radial Dysplasia

Eleanor M. Feneck [a], Jack Morgan [a], Ferheen Baig [b], Javier Barallobre-Barreiro [b,†], Fursham Hamid [c], Karla Lozano Gonzalez [c], Rosamund Nuamah [d], Shichina Kannambath [d], Pawan Dhami [d], Edel DeBuitleir [e], George R.F. Murphy [a,e], Branavan Sivakumar [e], Gillian Smith [e], Manuel Mayr [b,†], Malcolm P.O. Logan [a,*]

[a] Randall Centre for Cell and Molecular Biophysics. King's College London, Guy's Campus, London, United Kingdom
[b] King's British Heart Foundation Centre, King's College London, Denmark Hill Campus, London, United Kingdom
[c] Centre for Developmental Neurobiology, King's College London, Guy's Campus, London, United Kingdom
[d] Genomics Research Platform and Single Cell Laboratory Guy's and St Thomas' NHS Foundation Trust and King's College London, United Kingdom
[e] Department of Plastic and Reconstructive Surgery, Great Ormond St. Hospital for Children, London, United Kingdom

ARTICLE INFO

*Keywords:*
Fascia
Fibroblasts
Extracellular matrix
Radial dysplasia
Proteomics
Single-cell sequencing
Mechanobiology
Interleukin-6

ABSTRACT

Fibroblast cells are broadly distributed throughout the body and play instructive roles in tissue development and homeostasis. Defects in fibroblast function have been associated with developmental disorders, cancer and inflammatory disease. Our results reveal a previously unappreciated defect of fascial fibroblasts in patients with the upper limb congenital abnormality, Radial Dysplasia (RD). We identify compositional abnormalities in the extracellular matrix secreted by RD fascia-derived fibroblasts and provide an explanation for the consequent disorganisation and altered material properties of RD fascia and how this may impact disease pathology and patients' response to treatment. We show the abnormalities of RD fascial fibroblasts are reversible in vitro and identify a pathway with therapeutic potential to treat the soft tissue defects associated with RD. More broadly, our results have implications for understanding how heterogeneous tissue-resident fibroblast populations and the ECM they secrete contribute to normal tissue formation, homeostasis and disease.

## Introduction

A key function of fibroblasts is to secrete the extracellular matrix (ECM) that comprises tissue fascia, the material that provides structural integrity and continuity to individual tissues in the body and creates the boundaries between tissues. Recently, it has become increasingly clear that tissue fibroblasts are not simply generating a static, structural matrix into which the different cells of the body are embedded, but they also play critical signalling roles by modulating a dynamic ECM environment [1,2]. The effects of the ECM on cell signalling can be mediated by the degree to which signals can be sequestered or presented by the matrix milieu. Additionally, modifications to the physical properties (stiffness) of the matrix will influence the biophysical forces experienced by cells, which in turn affect cell fate and behaviour [3,4].

While originally considered a homogenous cell population, the application of new techniques such as single-cell transcriptomics has greatly accelerated the identification of diverse fibroblast populations throughout the body, not only between fibroblasts resident in different tissues but also within specific tissues themselves [3,5–8]. Given the importance of fibroblasts in the formation and homeostasis of a range of tissues and organs, it follows that disruption to fibroblast function is associated with disease. These include dermal and keloid scars, scleroderma, lung, heart and liver fibrosis, rheumatoid arthritis and ulcerative colitis [7,9–14]. In cancer, fibroblasts in tumours are known to secrete growth factors and can modify matrix and aid in metastasis [15,16]. Fibroblasts also secrete cytokines associated with inflammation [17–19]. The fibroblasts resident in muscle tissue are responsible for laying down the honeycomb-like myofascial scaffold that provides both structural integrity to muscle tissue and is critical in buffering and transmitting forces of contraction [20–23]. Skeletal muscle fascia has a 3

* Corresponding author.
*E-mail address:* malcolm.logan@kcl.ac.uk (M.P.O. Logan).
† Current address: British Heart Foundation Centre for Research Excellence, Imperial College London, White City Campus, United Kingdom.

https://doi.org/10.1016/j.matbio.2026.02.004
Received 28 November 2025; Received in revised form 3 February 2026; Accepted 26 February 2026
Available online 27 February 2026

layered architecture; the outermost epimysium encapsulates individual muscle bundles, the perimysium encases clusters of muscle fibres, into so called 'fascicles', and the endomysium surrounds individual muscle fibres [24]. The muscle fascia fibroblasts are primarily responsible for generating the ECM in muscle tissue and not muscle fibre cells [20,25]. The myofascial ECM is comprised of a diverse array of proteins that provide mechanical, biomechanical and signalling cues to surrounding cells. Each myofascial layer (epimysium, perimysium, endomysium) has its own unique composition of matrix proteins that reflect their specialised function [22,23].

During muscle tissue formation, the progenitors of the myofascial fibroblasts play an essential role in orchestrating the events that enable muscle fibres to coalesce into individual muscle bundles [26–28] and altered secretion of ECM proteins is associated with connective tissue diseases [29]. We have shown recently that the soft tissue abnormalities characteristic of an upper limb congenital abnormality, Radial Dysplasia (RD), can be explained by disruption in the normal activity of fascial fibroblasts [30]. In RD, the soft tissue and bony elements of the radial aspect of the forelimb are reduced or absent [31]. Since muscles normally attach to bone, it could be predicted that the absence of a muscle insertion site due to loss or reduction of a bone may lead to changes in the associated muscle and soft tissues or vice versa. In RD, however, there are frequently abnormalities in muscles where associated bones are unaffected. Furthermore, studies in mouse models have demonstrated that conditionally targeting the connective tissue fibroblasts can produce RD-like disruption of soft tissues in the forelimb without affecting bone formation [26,27]. In RD, deficiency of the radius ranges from hypoplasia to complete absence and can be accompanied by varying degrees of ulna bowing. The resultant wrist instability and malpositioning contribute negatively to limb function and cosmesis, thus impacting significantly on patient quality of life. There is currently no consistently reliable treatment intervention that can fully address RD defects and associated sequelae [32].

In this study, we carry out a proteomic and transcriptomic analysis of fascia-derived fibroblasts (FDFs) from the soft tissues of RD and control patients. The in vitro fibroblasts analysed in this study most closely resemble the epimysium. We identify novel diversity in this fibroblast population and identify gene expression changes associated with RD. We quantify changes to the material properties and reveal ultrastructural abnormalities in RD fascia that can explain the stiff soft tissues characteristic in RD and show they are consistent with changes in ECM composition we have identified with our 'omics' approaches. We conclude a disruption in the levels of collagen type III (COL3A1), tissue inhibitor metalloproteinases (TIMPs) and small leucine rich proteoglycans (SLRPs) secreted by FDFs contribute to the disrupted ECM which is ultimately responsible for the failed development of mature soft tissues in RD. Finally, restoring levels of interleukin-6 (IL-6) signalling in RD FDFs can improve the ECM organisation and composition, producing a matrix similar to control FDFs. We propose the IL-6 signalling pathway as a target for treatment strategies to address soft tissue defects in RD and potentially other connective tissue disorders.

## Results

### *RD FDFs secrete a compositionally abnormal extracellular matrix*

We have shown previously by immunohistochemical analysis that there are differences in the matrix secreted by RD FDFs compared to control FDFs [30] (Fig. S1). To carry out a comprehensive and unbiased characterisation of the normal FDF matrisome and the extent to which this is altered in RD, control and RD samples were analysed by LC MS proteomics (Materials and Methods, Fig. S5). Discovery analysis of the control FDFs matrisome identified the presence of 241 different proteins (Data S5) [33]. A selection of ECM proteins were verified with targeted proteomics analysis (Data S1 and Fig. S8). As expected, fibronectin (FINC) and collagen type I (alpha-1 chain (COL1A1) and alpha-2 chain (COL1A2)) (Fig.S5) proteins are detected, since they are known core components of the ECM. Additional structural constituents of the matrix are also present, such as the fibrillar collagen types III, V (COL3A1, COL5A2) and microfibril-forming type VI (COL6A1, COL6A2, COL6A3). There is an abundance of matrix-modifying proteins, such as matrix metalloproteinase-1 (MMP1), matrix metalloproteinase-2 (MMP2), metalloproteinase inhibitor 1 (TIMP1) and decorin, (Fig.S5). Gene ontology (GO) analysis indicates the control FDF matrisome is enriched in proteins involved with collagen cross-linking, organisation, tensile strength and ECM turnover (Fig.S6).

Comparison of the control and RD secretomes shows that most matrix proteins are abundant equivalently between control and RD samples but, amongst the proteins that do show altered abundance, the predominant change is a reduction in abundance in RD (Fig. 1A). Proteins that are reduced in RD ECM are functionally involved with structural organisation of the matrix and regulating collagen fibril diameter, matrix modification and basement membrane (Fig. 1C, Fig.S5–7). Collagen type III confers elastic properties to matrix and regulates collagen type I fibrillar morphology [34,35] and is downregulated in RD samples (Fig. S8), confirming our immunohistochemical observation of reduced collagen type III in RD myofascia [30]. Collagen type V is required for the physiological collagen fibril assembly of collagen types I and III [36, 37]. The SLRPs decorin and biglycan are reduced in RD (Fig. 1) and both are known to be expressed in myofascia in mature and forming muscle tissue [27]. Our proteomics results detect matrix modifying MMPs in FDF matrix (Fig.1). In RD samples, there is a reduction in matrix metalloprotease inhibitor 1 (TIMP1) abundance, suggesting an overall increase in MMP activity and matrix turnover in RD. We also observe downregulation of several markers of muscle basement membrane (laminin subunits and nidogen) suggesting muscle basement membrane alterations are associated with RD (Fig.1C). Gene ontology GO analysis of differentially abundant proteins classifies them into functional groups involved in ECM organisation, ECM turnover and collagen crosslinking (Fig.S6-S7). We also identify proteins with increased abundance in the RD secretome compared to control (Fig. 1). Procollagen C-endopeptidase enhancer 2 (PCOLCE2) and collagen type XIV (COL14A1) have roles in modulating collagen fibrillogenesis [38–40]. The synaptic remodelling protein neuronal pentraxin-1 (NPTX1), is also expressed in a variety of tissues including connective tissue cells [41]. Full statistical results are listed in Data S1.

### *Differential expression of genes in RD FDFs*

To further probe the normal gene expression signature of fascial fibroblasts and any transcriptomic changes in RD, we carried out single cell (SC) transcriptomic profiling of control and RD FDF cell lines using the 10X genomics platform (Fig.2). We previously demonstrated heterogeneity in the progenitor population of FDFs [27], therefore we looked for evidence of transcriptionally distinct fascial fibroblast subpopulations in our patient derived cell lines and if there are any changes in their distribution in RD. Cluster analysis of the sequencing data reveals four distinct clusters in control FDFs cell lines (Fig. 2A). These FDF subpopulations were identified across all 3 control cell lines and expresses distinct sets of gene markers (Fig. 2B and Fig. S9). Gene Ontology enrichment analysis of these cluster markers reveals that these genes are involved in glycosaminoglycan binding and ECM structure. Interestingly, cluster C3 is enriched with genes associated in chromosome organisation and chromatin remodelling (Data S2). Next, we compared the transcriptomes of these control FDF clusters to those identified in the human embryonic limb cell atlas [42,43] (Fig. 2C). Our cluster correlation analysis showed that clusters C1, C2 and C3 most closely resemble MFAP5+ fibroblasts while cluster C0 resembles STMN2+ fibroblasts. We identify genes that are both upregulated and enriched within the control clusters (Fig. 2A–B). Upregulated genes are involved in glycosaminoglycan binding and ECM structure. Specifically in cluster 3, enriched gene markers are associated with chromosome organisation

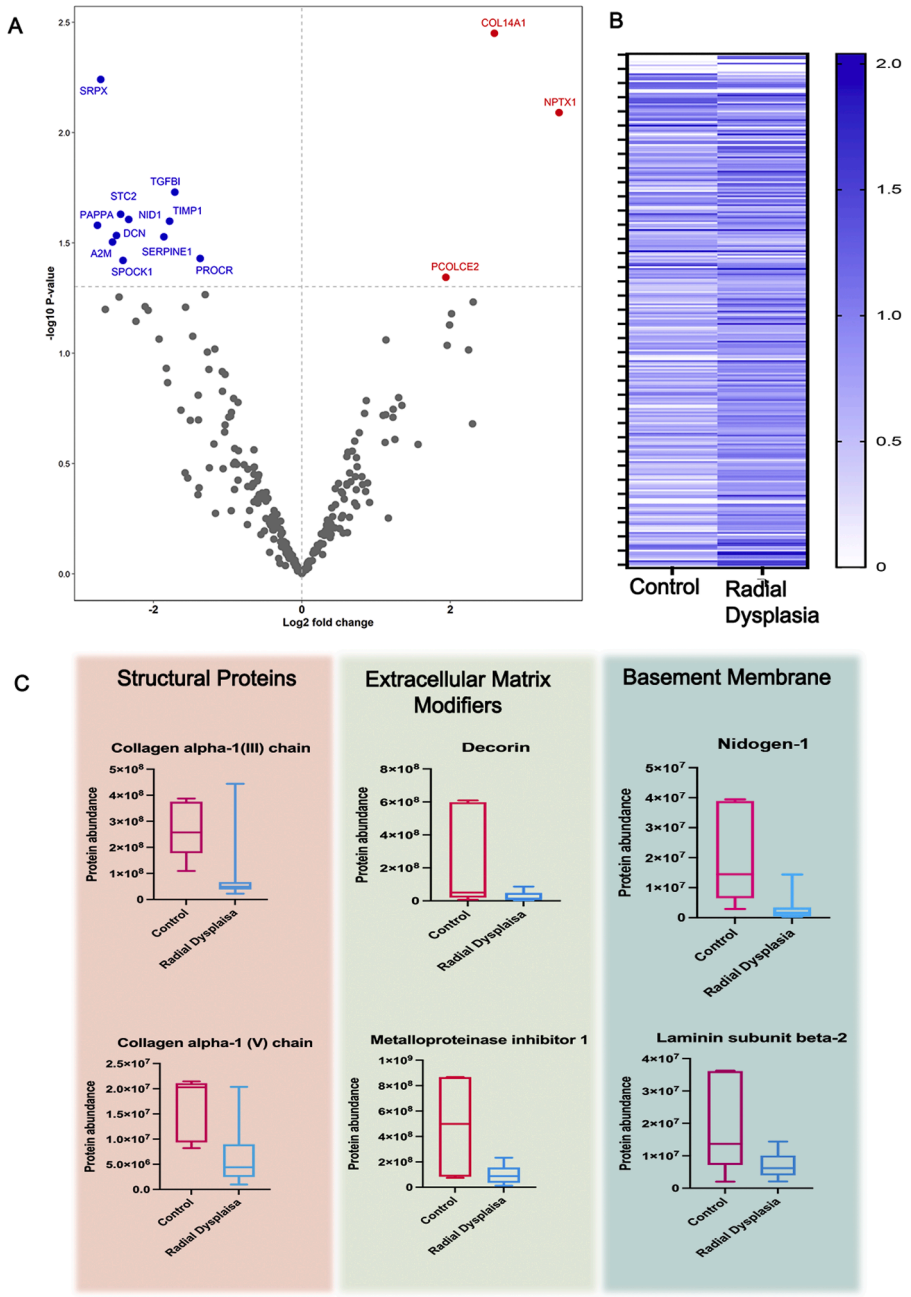


**Fig. 1.** Radial Dysplasia (RD) fascia-derived fibroblasts (FDFs) secrete a compositionally abnormal extracellular matrix. (**A-B**) Secreted ECM protein abundance of RD FDFs compared with control FDFs obtained by LC-MS analysis (**A**) Volcano plot showing downregulated and upregulated ECM proteins in RD FDFs compared to control. (**B**) Heatmap comparing control and RD FDF secretome protein abundance. **(C)** Box and whisker plots of the distribution of selected ECM proteins down-regulated in RD, grouped by their functional classification in the Matrisome database. The reduction in abundance of collagen type III (p-value 0.099) and V (p-value 0.054) and laminin subunit beta-2 (p-value 0.830) did not reach significance threshold with this discovery LC-MS analysis. Reduction in abundance of decorin (p-value 0.029), metalloproteinase inhibitor-1 (p-value 0.025), nidogen-1 (p-value 0.025) are statistically significant.

and chromatin remodelling (Data S2). We repeated the analysis on the RD patient cell lines and identified four distinct cell clusters (Fig. 2D–E).

Similarly, the transcriptome of cluster R0 closely resembles STMN2+ fibroblasts while clusters R1, R2 and R3 resemble MFAP5+ fibroblasts. Similarities in fibroblast subpopulations were also observed in both control and RD patients. Cluster R0 were mostly like cluster C0, clusters R1 and R2 resembled cluster C1 and clusters R3 resembled clusters C2 and C3. It is noteworthy that the gene MIR31HG was identified as cluster markers for both C1 and R1 while the PTX3 gene is found in clusters C0 and R3. These markers have also been described in clusters of embryonic limb fibroblast scRNAseq datasets [42,43] (Fig. 2C). GO analysis identifies gene markers within R2 that are involved in the inhibition of muscle growth, while enriched genes found in R3 have roles in inflammation, macrophage recruitment, downregulation of interleukins and cytokine recruitment (CXCL8,3,1,6 and CCL2) [44] (Fig.2D and Data S2).

We then performed differential expression analysis between RD FDF clusters and control FDF population to identify the RD FDF subpopulation that are most distinct and the genes that distinguishes these clusters from control FDFs. The results showed clusters R0 and R1 exhibiting markedly low expression levels of 9 and 4 genes, respectively (Fig. 2F). Gene ontology enrichment analysis using the PANTHER database [45]

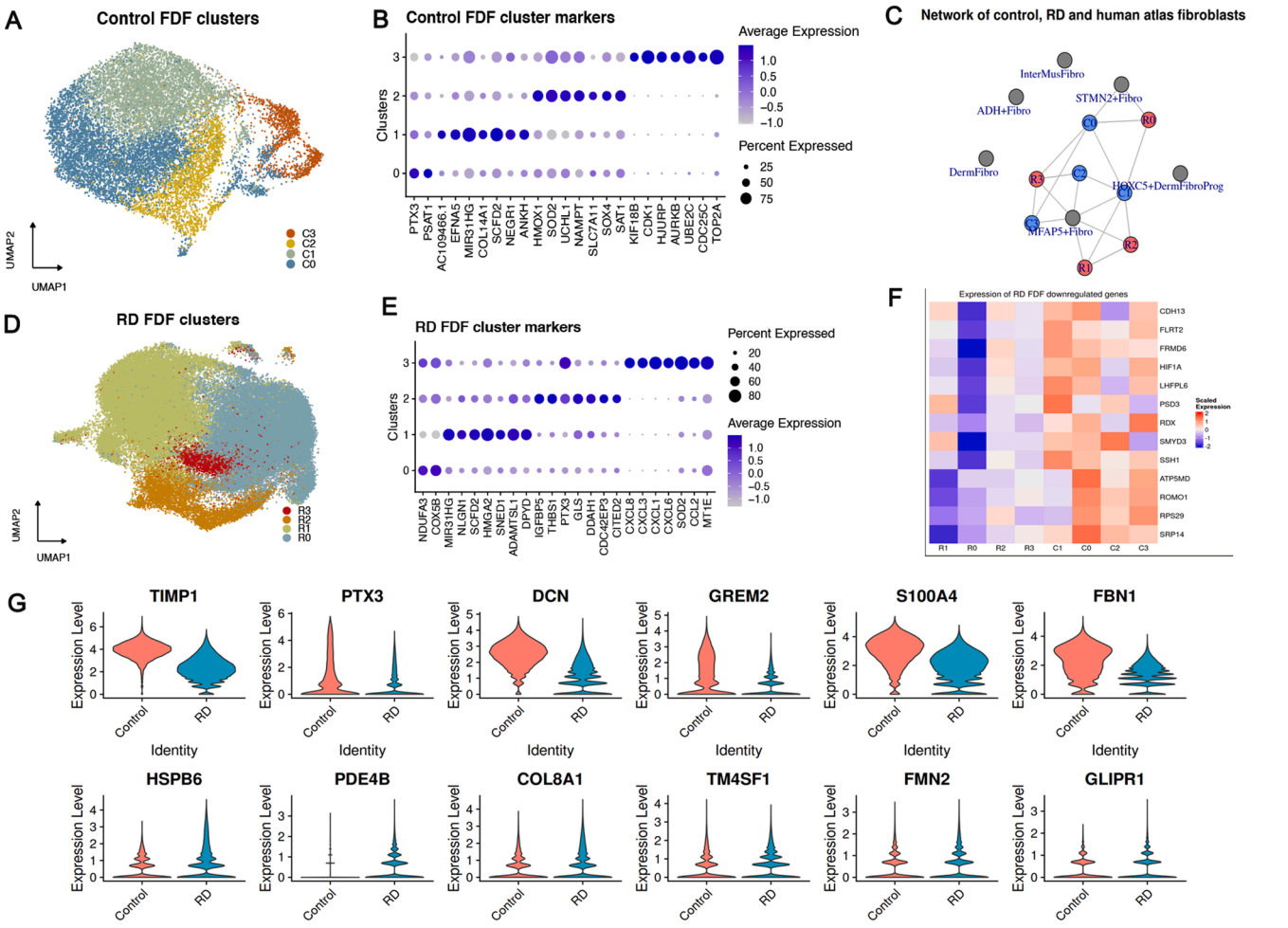


**Fig. 2.** Transcriptome single cell sequencing identifies differentially expressed genes in Radial Dysplasia (RD) fascial derived fibroblasts (FDFs). (**A**) UMAP of control FDF data identifies 4 clusters. (**B**) Dot plot showing the average expression and percent expressed of differentially expressed (DE) markers that characterise four clusters identified in control FDFs. (**C**) K-nearest neighbour graph showing similarities between the transcriptomes of fibroblast clusters from this study (red/RD and blue/control nodes) and those from Zhang et al. (39) (grey nodes). Control FDF clusters are shown as blue nodes while RD clusters are shown and red nodes. (**D**) UMAP of RD FDF data identifies 4 clusters. (**E**) Dot plot showing the average expression and percent expressed of differentially expressed (DE) markers that characterise four clusters identified in RD FDFs. (**F**) Heatmap comparing the expression of genes downregulated in RD FDFs in each of the 4 clusters identified control and RD clusters. (**G**)Violin plots showing altered expression of selected genes in RD FDFs (cyan) compared to control (red). Top row shows genes most significantly downregulated in RD FDFs compared to control. Bottom row shows genes most significantly upregulated in RD compared to control.

identifies these genes in controlling various aspects of cell behaviour. Genes downregulated in cluster R0 have roles in cell proliferation and migration (SMYD3, PSD3, FRMD6), cell adhesion (FLRT and CDH13), involvement in actin filament dynamics (SSH1 and RDX), angiogenesis (HIF1A) and mesenchymal differentiation (LHFPL6). These findings suggest RD fibroblasts within cluster R0 have reduced capabilities of classical fibroblast cell functions including adhesion, proliferation and migration. Downregulated genes in R1 associate with RNA metabolism, translation, protein synthesis and protein transfer (SRP14, ROMO1, RPS29, ATP5MD) suggesting fibroblasts within R1 have dysfunctional protein synthesis and transport. The enriched genes within each control and RD cluster are listed in Data S3.

Comparison of gene expression levels between combined population of RD and control fibroblasts reveals 2933 downregulated and 6 upregulated genes (Fig. 2G and Data S3). Many of these mis-expressed genes are associated with ECM protein degradation and organisation, consistent with the results of our proteomic analysis. Matrix metalloproteinase inhibitor-1 (TIMP-1) is downregulated. TIMP-1 is associated with tissue fibrosis and inflammation [46,47] and a reduction in expression would increase matrix metalloproteinases (MMPs) activity and further degrade matrix proteins. Other candidates provide tissues elasticity (fibrillin-1 and collagen type III) and maintain collagen fibril morphology and architecture (Decorin and Biglycan) (Fig.2I and Data S3). The reduction in collagen type III, collagen type V, decorin and TIMP-1 observed in the proteomic analysis was replicated in the transcriptomics results (Fig.2I and Data S3), providing independent verification and potential explanation for the decreased levels of protein we observe in the RD secretome (Fig.1).

Genes overexpressed in the RD transcriptome include collagen type VIII (Fig. 2I), a protein enriched in vascular smooth muscle, basement membranes, developing vessels, in tissues with porous networks, and during vascular injuries [48–52]. A knockout model of collagen type VIII increases tropoelastin and elastic fibre deposition and assembly [53]. Elevated expression of collagen type VIII in RD corelates with a reduction in elastic fibres in RD fascia. Differentially expressed transcripts specific to each RD cell line are listed in Fig.S10. The changes in protein and gene transcript abundance we have identified serve as biomarkers of RD, potential patient- and disease subtypes that have diagnostic and prognostic potential.

*RD patient fascia has altered mechanical properties, with areas of greater stiffness*

Our secretome analysis demonstrate that several proteins important for tissue elasticity and tensile strength are reduced in the matrix secreted by RD FDFs. For example, collagen type III is abundant in elastic tissues and its reduction in Vascular Ehlers Danlos Syndrome (Type IV) (vEDS) leads to the rupturing of vessels [54]. In addition, our transcriptomic data show fibrillin-1, an important glycoprotein in the biosynthesis of elastic fibres, is reduced in RD FDFs (Data S2). To directly test the mechanical properties of control and RD fascia, we used Atomic Force Microscopy (AFM) to measure tissue stiffness (Fig.3). AFM is being used increasingly to probe the micromechanical properties of soft tissues [55,56], but it has not previously been applied to human RD fascia. Measurements obtained from control samples fall into a range of values between sub-1 kPa - 70 kPa, with the majority between 5 - 15 kPa, broadly in line with values reported for other human tissues [57,58]. In contrast, RD fascia samples produced a greater range of Young's modulus values, from <1 kPa to 115 kPa (Fig. 3A) and a shift towards a peak of higher *E* values on the frequency distribution curve (Fig. 3A). In most RD samples, the average stiffness was greater than control fascia with some regions much stiffer. Comparing all 5 samples from both RD and control tissue, RD samples accounted for both the 2 lowest and 3 highest ($n$ = 5 samples per condition) overall mean sample stiffness values, highlighting the increased range and stiffness variability amongst different RD patients (Fig. 3B). This is further demonstrated by the greater distribution range and mostly higher mean values of the individual RD patient samples compared each individual stiffness map of control samples (Fig. 3C). Broadly, these data suggest that RD fascia has more heterogenous material properties than control fascia, with a greater range of stiffness values, and areas of comparably higher stiffness.

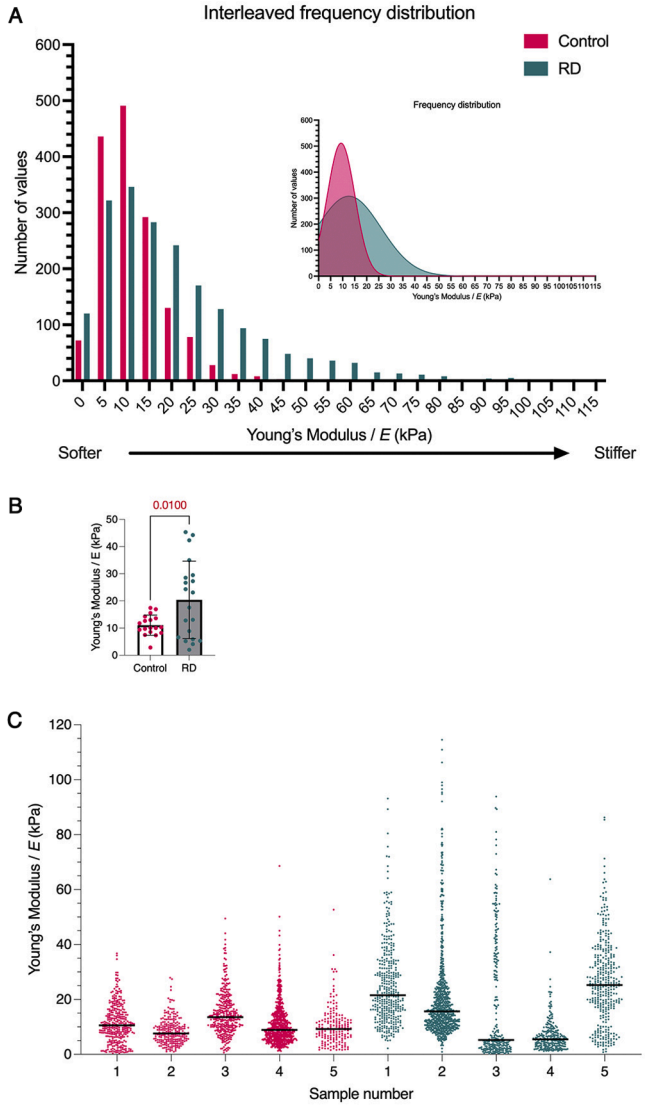


**Fig. 3.** Comparisons of Young's Modulus / E between RD and control patient fascial tissue biopsies measured by atomic force microscopy. **(A)** Bar graph of interleaved frequency distribution of Youngs modulus/*E* values (kPa) of control (pink) and RD (green) fascia biopsies. Note the wider range and comparably higher *E* values in the RD group, visualised in the nonlinear fit curves (**A**, inset). (**B**) Variation in average regional *E* values across all samples. Bar chart plotting the mean *E* value for individual force maps in control (pink circle) and RD (green circle) samples. Statistical significance (P value. $p$ = 0.0100) was determined by an unpaired *t*-test with Welch's correction. Error bars = mean with SD. (**C**) Scatter plots of combined maps Youngs modulus/*E* values (kPa) obtained from each of the 5 control patient (pink) and 5 RD patient (green) fascia samples analysed with black bars representing the median values from each patient sample.

*Collagen fibril diameter and spacing is disrupted in RD fascia*

The altered biomechanical properties of the fascia in combination with modified ECM protein composition suggest there is a change to the ultrastructural properties of RD fascia. These matrix constituents, such as collagen type III, collagen type V, decorin and biglycan directly regulate collagen fibril assembly and organisation [59–61], therefore we compared the ultrastructure of control and RD collagen fibrils using transmission electron microscopy (TEM) (Fig.4). In sections of control fascia, the regular spacing and compact arrangement of circular fibrils is evident (Fig. 4A–D), whereas in equivalent RD fascia collagen fibrils are more irregularly spaced and less densely packed (Fig. 4E–H). Measurements of control collagen fibril diameters range between 44.88–69.63 nm, consistent with dimensions described form other tissues [62]. RD collagen fibrils have a wider range of diameters (Fig. 4I). Similarly, there is a regular distribution of collagen fibril spacing in control collagen fibrils, while in RD collagen there is a greater distribution in fibril spacing distance (Fig. 4J). In some regions of RD fascia, collagen fibrils are bent or buckled (Fig. 4K, L). This abnormal morphology could result from the initial mis-assembly of collagen fibrils or be a secondary response caused by altered mechanical properties of the surrounding matrix. In summary, we identify defects in collagen fibrillogenesis, assembly, packing and organisation as features of the soft tissue pathology in RD and are likely a consequence of the altered ECM composition secreted by RD FDFs.

*The extracellular matrix environment alone cannot correct RD FDF function*

To explore the behaviour of the RD fibroblast population, we tested the effect of mixing different proportions of control and RD cells in co-cultures and measuring the resulting matrix organisation. Control FDFs were mixed in coculture with RD FDFs at a 1:1, 1:2 and 2:1 ratio and the organisation of the cell-derived matrix (CDM) quantified (Fig. S2A-E). We observe a general trend that the extent of disruption of matrix organisation is proportional to the amount of RD cells present in the culture (Fig.S4F). Furthermore, the presence of RD cells has a negative impact on matrix order, even when they represent a minority of the cell population.

To study the differences in cell behaviours between control and RD FDFs and to what extent this is influenced by the matrix substrate, we analysed the ability of control cells to organise when seeded on to (disorganised) RD CDM and, conversely, whether RD cells form a more organised network on matrix secreted by control cells. Ascorbic acid is an essential cofactor for collagen biosynthesis [63] therefore cells grown

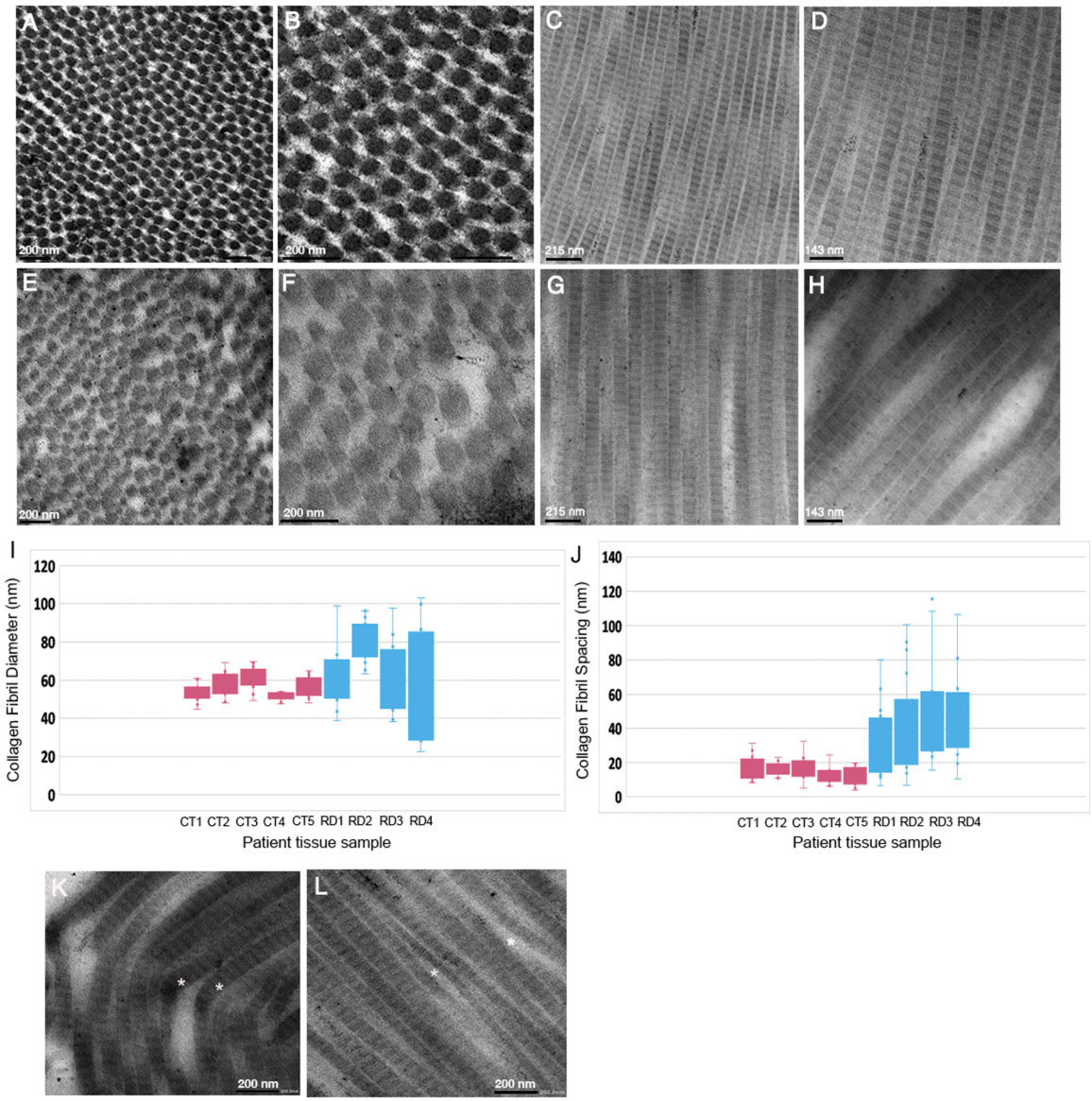


**Fig. 4.** Ultrastructural changes to collagen fibril organisation and morphology in Radial Dysplasia (RD) fascial tissue. Transmission electron microscopy (TEM) imaging of control (**A-D**) and RD collagen fibrils (**E-H**) in transverse (A,B,E,F) or longitudinal views (C,D,G,H,), respectively. Box and whisker plots of (**I**) collagen fibril diameter ($p < 0.05$) and (**J**) collagen fibre spacing ($p < 0.05$) measurements from 5 control (CT1–5) and 4 radial dysplasia (RD1–4) samples. **(K-L)** Collagen fibrils in RD tissue with a bent or kinked morphology (white asterisks), which are absent in control fascia (**C,D**).

on CDMs were cultured without the addition of ascorbic acid to minimise new collagen matrix production by the seeded cells impacting cell behaviours and CDM architecture. Control cells seeded on control matrix form organised, confluent parallel arrays of elongated cells (Fig. 5A). In contrast, control cells seeded on RD matrix are relatively disorganised (Fig. 5B), suggesting control cells are responding to the substrate and align along the comparatively disorganised matrix produced by RD cells. RD cells grown on control matrix can align along the CDM substrate to form organised arrays of cells in parallel (Fig. 5C). RD fibroblasts are therefore not inherently incapable of becoming aligned and can become more organised, if provided with the template of a normal, organised CDM substrate. However, amongst the population of RD fibroblasts grown on control CDM, gaps between some cells are consistently observed (Fig. 5C, asterisk), a feature that is consistently seen in RD FDF assays (Fig. 5D, asterisk). RD FDFs are unable to establish or maintain all the cell-cell attachments to form a confluent layer of cells even on control matrix, demonstrating, normalising the ECM substrate alone is not sufficient to correct this abnormal feature of RD fibroblast behaviour.

To further explore the functional differences between control and RD FDFs we tested whether cells plated onto CDMs can remodel this matrix under conditions where new collagen secretion is suppressed (absence of ascorbic acid in media). The distribution of collagen type I in CDMs was analysed after re-seeding with either control or RD FDFs (Fig. 5E–H) and the degree of collagen organisation quantified using Alignment by Fourier Transform [64] to generate order parameter values (Fig. 5I). ANOVA statistical analysis indicates all matrix order parameter values for remodelled CDMS are significantly different ($p = 0.0019$), with *t*-test results between control cells/control ECM vs control cells/RD ECM assay ($p = 0.0114$) and RD cells/control ECM and RD cells/RD ECM ($p = 0.0255$) (Fig. 5I). When control FDFs are plated onto control derived CDMs the matrix remains relatively organised (Fig. 5E). RD CDM order parameter values increase when seeded with control FDFs (Fig.5F). The CDMs produced from re-seeded RD cells grown on existing control CDM matrix produce a matrix with 'voids' (Fig5G asterisks) comparable to the RD CDM morphology (Fig. 5H).

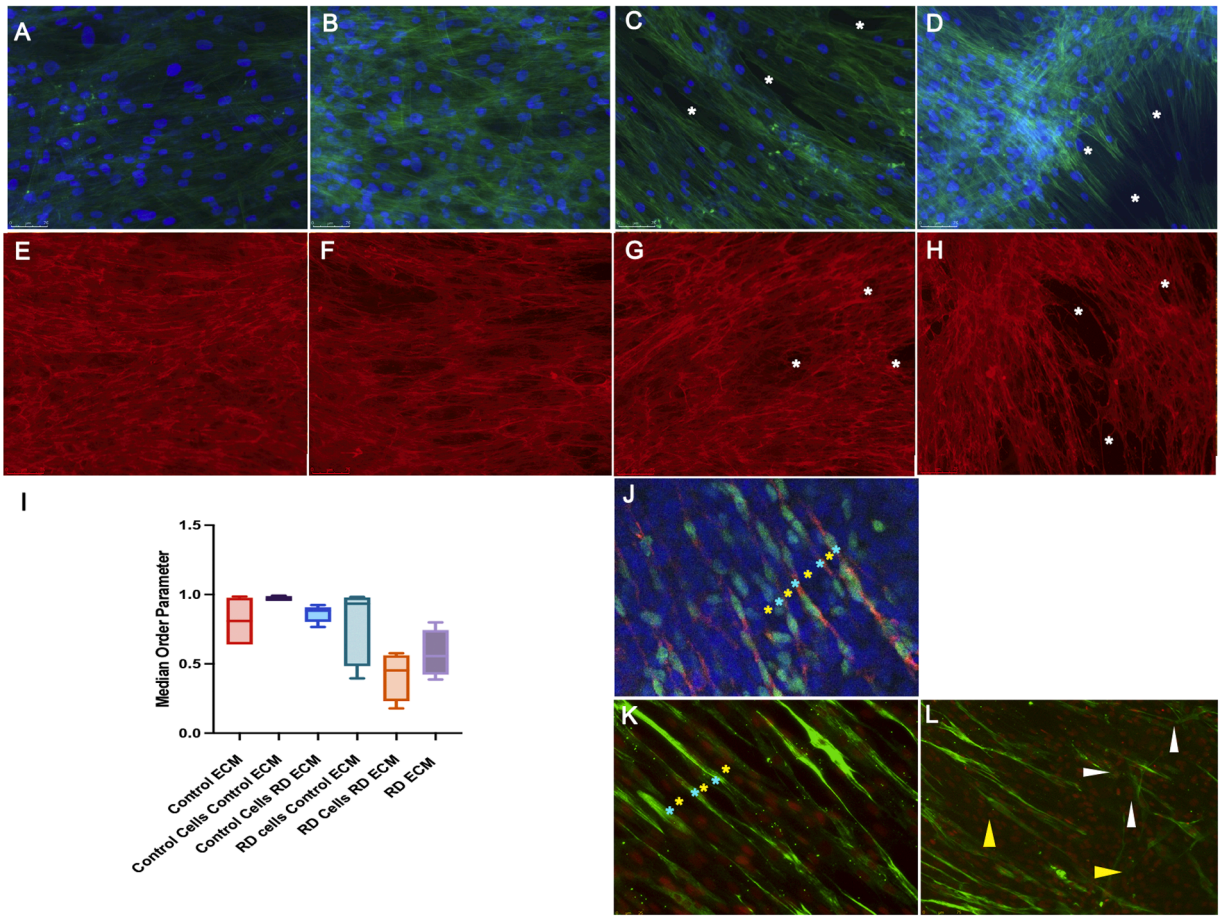


**Fig. 5.** Radial Dysplasia (RD) fascia-derived fibroblasts (FDFs) can disrupt normal extracellular matrix (ECM). (A-D) Fibroblast cells seeded onto normal or RD cell-derived matrix (CDM) in the absence of ascorbic acid (AA), cultured for 5 days and stained with Phalloidin (green) and DAPI (blue). (**A**) Control cells cultured on control CDM, (**B**) Control cells on RD CDM, (**C**) RD cells on control CDM and (**D**) RD cells seeded onto RD CDM. Acellular voids (asterisks) are present between neighbouring RD cells (**C,D**). (**E-H**) Collagen type I-stained CDM produced by the culture combinations described in **A-D**. Gaps in the ECM are present in RD CDM (**F, H** asterisks) and in control CDM after culture with RD cells (**G**, asterisks). (**I**) Box and Whisker plot of Fourier transform alignment analysis order parameter values of CDMs produced after culture conditions described on the x axis. (**J**) Confocal microscope image of muscle cells (myosin, red and myogenin, green) in an embryonic day E12.0 limb bud. Aligned, alternating muscle cells (blue asterisk) and fibroblasts (DAPI-positive nuclei, yellow asterisks). (**K**) Co-cultures of control muscle cells (GFP+) and control FDFs (red nuclei stain SPYDNA555) and (**L**) control muscle cells (GFP+) and RD FDFs (red nuclei stain SPYDNA555). (**L**) Cocultured muscle cells (GFP+) and RD FDFs are more disorganised (white arrows) and less aligned (yellow arrows). ANOVA indicates all matrix order parameter values for remodelled CDMS are significantly different ($p = 0.0019$), *t*-test results between control cells/control ECM vs control cells/RD ECM assay ($p = 0.0114$) and RD cells/control ECM and RD cells/RD ECM ($p = 0.0255$). All microscopy images at 20X magnification.

*FDFs and their secreted extracellular matrix can control muscle fibre alignment*

During the initial steps of muscle bundle formation in the mouse, precursor fibroblasts and muscle cells can be observed in regular, alternating lines of single cells (Fig.5J). This cellular arrangement is recapitulated in vitro when control FDFs and control muscle cells are plated together in co-culture, forming a pattern of alternating fibroblast-muscle-fibroblast cells (Fig. 5K, asterisks and Video S1). In co-cultures of the same control muscle cell line with RD FDFs, the muscle cells are less well aligned (Fig. 5L and Video S2) indicating that RD FDFs are unable to organise muscle cells to the same extent as control FDFs. Together these results are consistent with a model in which fibroblasts influence muscle fibre organisation by laying down an aligned ECM, and that the disrupted organisation of RD muscle tissue is caused by the relatively disorganised matrix laid down by the fibroblasts.

*Interleukin-6 (IL-6) can correct RD FDF cell and matrix alignment*

We observe a reduction of Il-6 protein in the RD FDF secretome (Fig. S3) and transcriptomic analysis identified reduced expression of IL-6 signalling downstream components, including STAT3/TIMP1/PTX3 (Fig. 2I and Data S3), indicating this pathway is downregulated in RD FDFs. We therefore tested the effect of exogenous IL-6 on RD FDFs and their secreted matrix. Control FDFs become aligned after 5 days in culture (Fig. 6A). In contrast, RD FDFs appear less aligned when cultured for the same time (Fig. 6C). Strikingly, following IL-6 treatment, RD FDFs have greater alignment (Fig. 6D), similar to that seen in control and control IL-6-treaetd cultures (Fig.6B). In RD cultures there are also irregularly spaced gaps between cells, reflecting less homogeneity in cell distribution and an apparent inability to form a confluent monolayer (Fig. 6C, see also Fig. 5C–D). After IL-6-treatment, RD cells form a more homogenous confluent monolayer (organisation assay between RD untreated and RD treated $p = 0.0025$) (Fig. 6D). A similar, but less marked effect, is observed following IL-6 treatment of control cells (Fig. 6B). Trajectory analysis of time-lapse recordings indicate that cell displacement is increased following IL-6 treatment of control cells (Fig. 6E–F&I-J, and Videos S3–6). RD cultures are less homogenous, with some cells showing little or no displacement during the culture period (Fig.6G&K). Following IL-6 treatment, RD cells have displacement trajectories that are similar to control and IL6-treated control cells (Fig.6H&L). To examine the potential compositional effects of IL-6 on the matrix and to

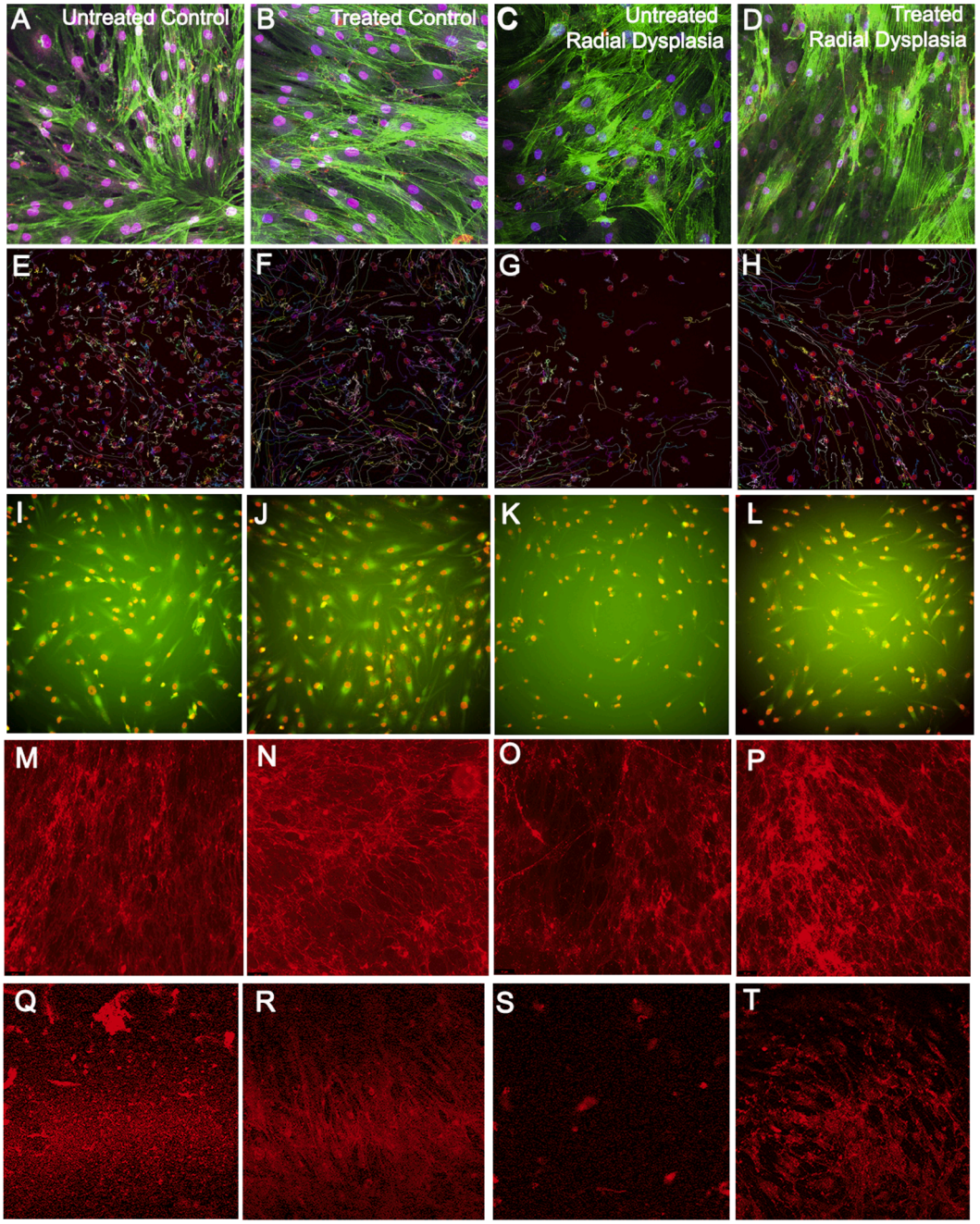


**Fig. 6.** Interleukin-6 (IL-6) treatment restores cell and extracellular matrix alignment of radial dysplasia (RD) fascial-derived fibroblasts (FDFs). Analysis of control and RD cells (**A-L**) and the CDM they secrete (M-T) with or without IL-6 treatment ($p = 0.0025$) (**A-D**) Phalloidin (F-actin) and SpyDNA555 (nuclei, pink) stained FDFs showing cell alignment and morphology. (**E-H**) Cell trajectory analysis of time-lapse imaged cultures. Fibroblast cells were imaged over a 60-hr period, +12 hrs after seeding. Nuclei were tracked with FIJI Trackmate. (**I-L**) Still images of time-lapse imaged cell cultures live-labelled with cytoskeletal BioTracker (green) and SpyDNA555 (red) dyes. (**M-T**) CDMs produced following culture conditions described in A-L for 3 days, processed and immunostained for collagen type I (**M-P**) or collagen type III (**Q-T**). All microscopy images at 20X magnification.

correlate this with changes in cell behaviour, we carried out immunohistochemical analysis of specific ECM proteins secreted by treated and non-treated cells. Collagen type III secretion is reduced in matrix produced by RD FDFs (Fig. 6S) but is detected in RD FDF matrix following IL-6 treatment (Fig. 6T). In summary, in all our observations, IL6 treatment restores RD FDFs alignment, cell behaviour and secretion of collagen type III (Fig. 6 and video S3–6).

## Discussion

This study provides multiple lines of evidence that dysfunctional fibroblast behaviour underlies the soft tissue pathologies of the disease, Radial Dysplasia (RD). We use a multi-disciplinary approach to identify novel changes to ECM composition, organisation, material properties and cell behaviours that provide explanations for the variable clinical presentation, pathology and disease progression of RD. We propose that strategies which can correct abnormal behaviours of RD fascial fibroblasts, by restoring fibroblast cell alignment, ECM organisation and

composition and ultimately the normal range of matrix stiffness, could improve treatment outcomes. Moreover, we demonstrate that the abnormal behaviours of RD fascial fibroblast can be reversed in vitro and provide evidence that modulation of the IL-6 pathway has therapeutic potential. We show how disease can be caused when the activity of a heterogeneous, tissue-resident fibroblast population is disrupted and how this could contribute to disease pathology during the life course and impact treatment regimes.

During embryogenesis, the FDF progenitor population orchestrates the process by which nascent muscle fibres form individual muscle bundles [20,26,27,29]. We propose that the abnormal properties we describe in FDFs obtained from paediatric RD patients are a continuum of abnormalities present in the progenitor population of these cells, and that similar changes in ECM composition, matrix disorganisation and subsequent mechanical properties to the matrix at embryonic stages, underly the aetiology of the soft tissue defects associated with RD [30,31,65]. Variations in the extent of these progenitor cell abnormalities could explain the variable presentation seen across affected individuals and between the different genetic syndromes that can all present with the clinical features of RD.

The changes we describe in RD ECM composition can explain the changes in matrix organisation and stiffness that we observe, both *in vitro* with RD FDFs and in patient tissue. In RD matrix, there is a significant reduction in proteins that maintain collagen type I architecture, including collagen types III and V, Decorin (Dcn) and Biglycan (Bgn) (identified in single cell sequencing and proteomics results) [61,66]. The disruptions in collagen fibrils in RD patients are similar to those described in humans with collagen type III mutations [60] and in mouse *Dcn/Bgn* double mutants [59,61]. Decorin influences collagen architecture by regulating collagen fibril lateral growth within tissues and is required for regular collagen fibril spacing and organisation [66–69]. We propose the altered collagen fibril diameter and spacing in RD fascia is a consequence of reduced collagen type III, collagen type V and SLRP levels secreted by RD facial fibroblasts. These findings are consistent with observations in other diseases, such as corneal stromal dystrophies and osteoarthrosis [67–70], where reduction of SLRP expression disrupts collagen structure. RD FDFs secrete less, TIMP-1, a broad-spectrum inhibitor of MMPs, which would cause an overall increase in MMP activity, increased matrix turnover and reduced ECM protein levels.

We identify significant disruption in collagen ultrastructure in RD, with variations in collagen fibril diameter, spacing and alignment. We suggest the decreased levels of collagen types III, V, Dcn and Bgn disrupt the physiological assembly of collagen fibres, contributing to the overall increased range of stiffness of the fascial tissue. “Tight” fascia and “stiff” wrist and elbow joints are commonly reported in RD cases [32,65,71] and could be caused by either the relatively stiffer or softer sub-regions of ECM/fascia we have measured (Fig.3). Imbalance of the musculature and stiffer soft tissues are likely culprits for the radial-deviated, partially flexed hand position and bowed ulna that commonly presents in RD. Furthermore, differences in the extent of excessive fascia stiffness between individual RD patients could explain the variable recurrence of radial deviation seen after surgical treatment which is performed with the aim of improving wrist alignment and maintaining long-term stability [32,65,71]. A deeper understanding of the mechanical properties of RD patient myofascia could improve diagnosis and help which patients are more likely to experience recurrence, thereby informing surgical planning and optimising outcomes. Measuring tissue stiffness in different forelimb muscles of RD patients prior to surgery using non-invasive elastography techniques could be helpful for assessing the patient’s suitability for surgery and chance of recurrence [72]. Therapeutic interventions that restore ECM composition and tissue biomechanics have the potential to improve treatment strategies. In this context, we suggest assessment of an individual patient’s soft tissue biomechanics may provide valuable guidance for determining the optimal treatment strategy.

Single cell transcriptomic analysis revealed a heterogeneous FDF population in both control and RD patient cell lines. We identify a unique RD cluster (RD3) with an inflammatory signature, with an increase in CXCL and CCL markers (CXCL8,3,1,6 and CCL2). This fascial fibroblast subpopulation could be primarily responsible for RD pathology, identifying changes to the inflammatory signature between RD and control FDFs. This result may influence the migration and function of immune cells such as macrophages in tissue development and repair. In addition, we identify changes in genes related to cell adhesion (FLRT and CDH13) and cell recruitment (SMYD3, PSD3, FRMD6), identifying a shift in gene markers which alter the ability of cells to communicate and behaviour coherently. Further studies that classify differences between cluster populations could have diagnostic and prognostic value in classifying the severity of RD pathology and response to treatment.

IL-6 is a cytokine involved in a variety of biological processes influencing fibroblasts, including wound healing and fibrosis. IL-6 has roles in matrix turnover; IL-6 can increase collagen type I and fibronectin secretion, reduces MMP activity and modulates collagen type III turnover [73,74]. IL-6 activates TGF-$\beta$ signalling, which in turn stimulates Dcn and collagen type III expression (Juhl et al., 2020). IL-6 knockout mice have reduced collagen deposition during wound healing [75] and deficiencies in TGF-$\beta$ signalling have been linked with the connective tissue disease Loeys-Dietz Syndrome [76]. IL-6 produced by muscle cells is a “myokine” that stimulates myogenesis and muscle hypertrophy [77]. In contrast to its effects in other sites of the body, IL-6 has anti-inflammatory effects in muscle [78,79]. Recent studies have shown that IL-6 can influence fibroblast cell alignment. IL-6 is upregulated in highly aligned dermal fibroblasts derived from keloid scars, with IL-6 increase linked to enhanced N-cadherin expression and contact inhibition [80]. We have previously reported a reduction of membrane N-cadherin in a Tbx5 mouse mutant model of Holt-Oram syndrome (HOS) that phenocopies RD-like limb defects [26], consistent with cell-cell adhesion defects in RD. Together this support a role of IL-6 in cell alignment, adhesion and ECM deposition, which are disrupted in RD FDFs. We observed a reduction in secreted IL-6 combined with reduced expression of IL6-signalling pathway components in RD FDFs. Our results suggest reduced IL-6 signalling through the STAT3 pathway in FDFs is associated with RD FDFs inability to form aligned cells and organised ECM. IL-6 treated RD fibroblasts increases the secretion of extracellular matrix proteins, restoring the secretion of collagen type III. Treatment strategies that can restore physiological levels of IL-6 signalling in FDFs could reduce disease progression and rates of recurrence following surgery.

In summary, this study reveals how disruption of fibroblast activities contribute to disease pathology and advances understanding of the roles of fibroblasts in healthy and diseased states. Our observation of abnormalities in fascial fibroblasts in paediatric cases has significance for how diagnostic, prognostic and treatment strategies can be approached. We propose that in RD, abnormal fascial fibroblast activity in the upper limb contributes to both clinical presentation at skeletal maturity and to recurrence of radial deviation after surgical interventions aimed at realigning and stabilising the wrist. The fact that we can reverse abnormal FDF behaviour in vitro demonstrates the potential that a similar restoration of normal fibroblast behaviour can be achieved in patients, which could reduce recurrence of radial deviation, tissue stiffness and improve treatment outcomes.

## Experimental procedures

### *Tissue collection*

Tissue collection and experiments were all carried out in compliance with the principles outlined in the World Medical Association declaration of Helsinki. The project was adopted by the UK National Institute for Health Research (NIHR) to their national research portfolio, with the Clinical Research Network ID 20,411. Ethical approval was granted by the London Hampstead research ethics committee (REC reference 15/

LO/2085). NHS Research and Development approval was granted from the recruiting hospitals. Tissue samples were collected with informed written parental (and where age appropriate, patient) consent.

Tissue biopsies from patients undergoing elective surgery were taken during surgery. Samples used for cell culture were placed in individual sterile containers and processed immediately after transportation to Guy's Campus, King's College London. Biopsies were processed depending on specific experiment requirements outlined within the methods. This study focuses on the soft tissue defects of RD; therefore, we did not collect or analyse bony tissue.

*Cell dissociation and culture*

Cell lines (10 RD and 8 control/non-RD patient-derived) were established using a method described previously [30]. Patient clinical presentation and tissue origin is listed in Table 1.Cells were expanded in fibroblast growth media (FGM) (Dulbecco Modified Eagle's medium (Gibco, Thermo Fisher), 10 % Foetal Bovine Serum (FBS) (Gibco, Thermo Fisher), 1 % Penicillin/Streptomycin (Gibco, Thermo Fisher), 1 % GlutaMAX (Gibco, Thermo Fisher) and 1 % Sodium Pyruvate (Gibco, Thermo Fisher)) incubated at 37 °C with 5 % $CO_2$, with media changed every 2–3 days. All cell lines analysed in this study were between passage number P4-P6.

*Proteomics*

The secretome of FDFs from RD patient cell lines (Table 1) were processed and analysed essentially as described [9]. Cells were cultured until ~60–80 % confluency. Cells were then moved to serum-free medium and left for 1 hr. before fresh serum-free medium was replaced. Cells were then incubated in serum-free culture medium for 72 h. The supernatant was centrifuged at 3000 g for 10 mins and 2 ml collected.

**Table 1**
Radial Dysplasia patient samples.

| Cell Line | Patient Presentation | Tissue of Origin | Sex (M/F) | Age (years, tissue collection) |
|---|---|---|---|---|
| RD1 | Townes-Brocks Syndrome | Flexor Carpi Radialis Sub-Sheath | M | 2 |
| RD2 | Spontaneous RD | Flexor Carpi Ulnaris Fascia | M | 16 |
| RD3 | VACTERL | Extensor Carpi Radialis Longus/ Brevis Fascia (distal retinaculum) | M | 5 |
| RD4 | VACTERL | Ulnar Fascia Over Abductor Digiti Minimi | F | 8 |
| RD5 | VACTERL | Flexor Carpi Radialis Fascia | M | 1 |
| RD6 | Holt-Oram Syndrome | Flexor Carpi Radialis Fascia | M | 3 |
| RD7 | VACTERL | Fascia from Thumb | M | 3 |
| RD8 | Thumb Hypoplasia | Fascia from Thumb | F | 2 |
| RD9 | VACTERL | Flexor Carpi Radialis Fascia | F | 4 |
| RD10 | Spontaneous RD | Dorsal Fascia | Not recorded | Not recorded |
| C1 | Control | Flexor Carpi Radialis Fascia | F | 9 |
| C2 | Control | Wrist Deep Fascia | M | 18 |
| C3 | Control | Flexor Carpi Radialis Fascia at Wrist | Not recorded | Not recorded |
| C4 | Control | Fascia Flexor Carpi Radialis | M | 12 |
| C5 | Control | Fascia from Thumb | M | 1 |
| C6 | Control | Fascia from Thumb | F | 1 |
| C7 | Control | Fascia from Thumb | M | 3 |
| C8 | Control | Fascia from Thumb | M | 10 |

Supernatant samples were concentrated using Amicon® Ultra 0.5 mL 3 kD Centrifugal Filters, according to supplier's instruction, yielding 20 ul concentrated protein sample after filtering. Protein concentration for all samples was measured and then processed in a stepwise series of 2-step deglycosylation (top remove glycan to aid identification of ECM proteins by LC-MS) in-solution denaturation, reduction, alkylation and trypsin digestion.

For discovery proteomics, separation was achieved on a nanoflow LC system (DionexUltiMate 3000 RSLC nano). Spectra were collected from an Orbitrap mass analyser (Q Exactive Plus, Thermo Fisher Scientific) using full MS mode (resolution of 60,000 at 200 $m/z$) over the mass-to-charge ($m/z$) range 350–1600. Data-dependent MS2 scan was performed using the top 15 ions in each full MS scan (resolution of 15,000 at 200 $m/z$) with dynamic exclusion enabled.

Data was searched against the human and bovine databases (UniProtKB/Swiss-Prot version from January 2021, 20,396 / 6004 protein entries, respectively) using Mascot (version 2.6.0, Matrix Science). The mass tolerance was set at 10 ppm for precursor ions and 20 mmu for fragment ions. Correlation of peptides for each protein was checked and peptides not reaching a threshold of 0.6 were not used for final quantitation. Sum of peptides was used for quantitation. Peptides were normalised using sum of total features. Proteins present in less that 30 % of samples were disregarded. The average protein compositions in the RD samples and the control samples were calculated A logarithmic fold change ($Log_2$) calculation determined the reduced change in the RD samples compared to the control samples. Statistical analysis was carried out in graph pad prism. A D'Agostino and Pearson normality test was conducted on all proteins. If a normal distribution was found, a parametric two-tailed $t$-test was conducted. If the distribution was not normal, a Mann-Whitney U test was conducted. Results were deemed statistically significant if the p-value was $<0.05$. Gorilla Go analysis was performed. A full protocol is available on request.

A PRM method was developed with the help of Skyline software (version 20.2.0.343, MacCoss Lab Software). Data from the untargeted analysis was used to select proteotypic peptides of ECM proteins selected by the collaborator. Due to the nature of the samples, it was ensured that peptides selected for PRM analysis were unique to human and not common for both human and bovine. Skyline was also used to optimize retention times. Proteotypic peptides were scheduled using the retention time obtained from test experiments with the same LC configuration and eluting gradient; retention time windows were set at ± 4 min. A total of 91 peptides were selected for the quantification of 27 proteins. After initial testing, samples were quantified for a final total of 88 peptides for 27 proteins (see list below).

| | |
|---|---|
| **BGH3_HUMAN** | **LAMC1_HUMAN** |
| **CCN1_HUMAN** | LTBP2_HUMAN |
| **CCN3_HUMAN** | LYOX_HUMAN |
| **CO3A1_HUMAN** | NID1_HUMAN |
| **CO5A1_HUMAN** | NID2_HUMAN |
| **CO5A2_HUMAN** | PGBM_HUMAN |
| **COEA1_HUMAN** | PGCA_HUMAN |
| **CSPG2_HUMAN** | PGM1_HUMAN |
| **ECM1_HUMAN** | PGS1_HUMAN |
| **FBLN3_HUMAN** | PGS2_HUMAN |
| **LAMA2_HUMAN** | SPON1_HUMAN |
| **LAMA4_HUMAN** | TARSH_HUMAN |
| **LAMB1_HUMAN** | TSP1_HUMAN |
| **LAMB2_HUMAN** | |

Spectra were collected from an Orbitrap mass analyzer (Q Exactive Plus, Thermo Fisher Scientific) using PRM mode (MS2 resolution of 30,000 at 200 $m/z$). An isolation window of 2.0 $m/z$, automatic gain control (AGC) values of 2E5 and a maximum injection time of 60 ms was used. Fragmentation was performed with a normalized collision energy of 28 and MS/MS scans were acquired with a first fixed mass of 110.0 $m/z$.

Using Skyline software, the identity of a specific peptide was confirmed by the presence of multiple transitions at the same retention

time. All peaks were reviewed and integrated manually. Total fragment peak areas were used for quantification of each peptide. A minimum of three fragments and a signal to noise level of 3 to1 was required for each peptide in order to qualify as quantifiable. Data were exported to excel for further data processing. After check peptide correlations, the sum of all viable peptides per protein, was used to quantify each protein. Data were normalised using the total sum of all features for each sample from MS1 data in Proteome Discoverer.

*Single cell RNA sequencing (ScRNA-seq)*

Cells were grown in a cell culture T175 Nunc EasYflask (ThermoFisher) for 3–5 days in FGM until 70–80 % confluence, all cell lines analysed were between passage number P4-P6. Cells were trypsinised and centrifuged at 3000 g for 3 mins, aspirated and washed with DPBS. Cells were further centrifuged twice and filtered using a cell strainer 40 mm Nylon (BD Falcon) into a FACS tube on ice. DAPI was added to the tube and cells were sorted using FACSAria 3 (BD biosciences, USA) to discard any DAPI+ cells. Cells were further quality checked and counted, cDNA generated (library generation) and stored at −80 °C until sequencing. All 9 cell lines (3 control and 6 RD) were tagged with a unique barcode and then pooled and sequenced together with 3′ single-cell transcriptomics.

Single cell suspensions from each sample were processed using Chromium Next GEM Single Cell 3′ Kit v3.1 assay for library preparation, according to the manufacturer's protocol (10x Genomics, USA) at recommended loading concentrations. cDNA generated from each sample was converted into dual indexed gene expression libraries and sequenced on the Illumina NextSeq 2000 System platform using a P3 (100-cycles) sequencing kit (Illumina, USA). A minimum of 20,000 reads/cell were generated for gene expression libraries. Raw sequencing data was converted into FASTQ files and processed using CellRanger v7.1.0 (10x Genomics, USA) and count matrix files were generated.

*Single cell sequencing analysis*

Short reads from the single cell sequencing data were aligned to the GRCh38 transcriptome using the CellRanger software (cellranger v7.1.0). Gene count matrices of each biological sample were then individually imported into R and analysed using the Seurat package (Seurat v4.1.3). Quality control was performed to retain cells expressing at least 100 genes and not >10 % of its transcriptome being mitochondrial genes. Normalisation of counts data and regression of cell cycle genes were performed using the SCTransform function. Fascia-derived fibroblasts from each sample were then combined based on the patient diagnosis (control and RD) using the Harmony package (v.1.2.3) followed by further reduction of the embeddings using UMAP and tSNE algorithms. This data integration and dimensional reduction process was repeated on all cells to obtain a unified dataset of all FDFs in this study. Clusters of FDF subpopulation was obtained using a graph-based clustering method. Firstly, a shared nearest neighbour graph was constructed using the Harmony-integrated embeddings as input. Cell modules were then identified using the Louvain algorithm at increasing resolution and the optimal resolution was chosen using the sum of squares method. Differential gene expression analyses were performed using Seurat's FindMarkers function. Specifically, the MAST framework was employed on normalised gene counts, and the sample ID grouping was used as the latent variable to account for patient-specific expression patterns. Cluster-defining markers are defined as genes showing an adjusted statistical significance of <0.05 and being expressed in at least 50 % of the cells.

*Immunohistochemistry*

Biopsy samples of fascia and muscle were flash frozen in liquid nitrogen and stored at –80 °C, cryo-sectioned (Leica) at 10 μm and sections placed on 'Superfrost® Plus' slides (ThermoFisher). Sections are circled with a hydrophobic pen and hydrated with phosphate buffered saline 0.1 % tween (PBST) solution. Primary antibodies were applied to the sections overnight at 4 °C at specific dilutions for each antibody (Table 2). Unbound primary antibodies were washed off 3x over 30 mins with PBST and secondary antibodies applied at desired dilution (Table 2). Secondary antibodies were left for 2 h at room temperature and subsequently washed with PBST. DAPI (1:1000 dilution stock 1mg/ml) was applied to sections for four mins before PBST washing and cover slips added with a mounting medium. All sections were imaged with a Leica DMi8 microscope or Nikon A1 inverted confocal microscope at X20, X40, X60 and X100 magnifications.

*Cell mixing*

FDFs were grown in FGM media until 80 % confluence. Cells were washed 2x with DPBS and 0.05 % trypsin added to create a cell suspension. Cells were pelleted by centrigugation at 3000 g for 3 mins; supernatant was aspirated and cells resuspended for cell counting using a haemocytometer. Cells were seeded (30,000 cells per well) in an 8-well plate at 100 %, 1:1, 1:2 and 2:1 control to RD cells for each cell line. Cells were grown for 5 days in the presence of 0.25nmol/L ascorbic acid (AA) in 10 % FBS and then decellularized. For decellularization, 20 mM Ammonium hydroxide 1 % Triton-X100 was added to each well for 5 mins and then diluted 1:1 with PBS and left in the fridge overnight. Once cells had detached from the plate, the cell derived matrix (CDM) was fixed with 4 % PFA and stained with collagen type I following the immunohistochemistry method (Table 2). CDMs were imaged with a LeicaDMi8 microscope and organisation quantified using a Fourier transform algorithm MATLAB script [64]. For quantification of order parameter values were obtained from a minimum of 3 areas of a single well and 8 wells per culture condition and cell lines (6 RD and 3 control cell lines).

*Atomic force microscopy (AFM)*

AFM, performed at the London Centre for Nanotechnology (UCL), was used to measure the Young's modulus ($E$) of control and RD fascial samples. Measurements were generated using a JPK CellHesion 200 AFM mounted on a motorised precision stage equipped with an inverted Olympus IX73 microscope. All equipment were placed on an active anti-vibration table (TMC) in an isolation chamber. JPK Scanning Probe Microscopy (SPM) software 5.0 (JPK Instruments) was used to control the AFM.

Tipless silicon nitride MLCT-O10 cantilevers (Bruker) were mounted

**Table 2**
Primary Antibodies.

| Antibody | Supplier | Protein detected | Dilution |
|---|---|---|---|
| Ab138492 | Abcam | Collagen Type I | 1:400 |
| Ab6310 | Abcam | Collagen Type III | 1:100 |
| Ab6586 | Abcam | Collagen Type IV | 1:100 |
| Ab7046 | Abcam | Collagen Type V | 1:100 |
| Ab182744 | Abcam | Collagen Type VI | 1:100 |
| F59 | Developmental studies hybridoma bank | Myosin | 1:50 |
| MF20 | Developmental studies hybridoma bank | Myosin | 1:50 |
| MY32 | Sigma | Myosin | 1:800 |
| EPR4789 | Abcam | Myogenin | 1:200 |
| 1G4 | Novus Bio | TCF4 | 1:200 |
| Phalloidin-FITC | Torcis Bioscience | Actin Phalloidin | 1:500 |

with 50 μm polystyrene beads (COUNT-CAL™ Particle Size Standard, CC50, Freemont, CA, USA) using UV-curable glue on cantilever 'F'. Beaded cantilevers were selected for use if the measured spring constant (k) was within the manufacturers accepted range (0.3 – 1.3 N/m). Bead-mounting and calibration was performed as per Norman et al. (2021) on a glass slide, and the F cantilever was selected through optimisation measurements using different cantilevers on sample tissue.

Flash-frozen tissue biopsies were cryosectioned at 10 μm and mounted on 'Superfrost® Plus' slides. Cryosections were thawed and a hydrophobic ring drawn around the sample with a PAP pen. Samples were washed, re-hydrated and measured in PBS at room temperature. Indentations were performed in 10 × 10 grids across 100 $\mu m^2$ on tissue regions. At least 4 grids were measured per sample and multiple sections from the same sample were used where feasible. A substrate validation was performed alongside to rule-out contributions to Young's modulus from the underlying glass.

Force-distance curves were generated in 'JPK/SPM data processing' software. The 'Hertz-fit' function was selected, tip radius entered manually (25 μm) and Poisson ratio set to 0.5. Force curves were accepted if they demonstrated a minimum indentation of 0.1 μm, with a minimum travel (the distance the beaded cantilever tip travels before contacting tissue) of 0.5 μm to exclude adhesion artefacts. Force curves were also rejected if they demonstrated breakage events, did not achieve a constant baseline or were noisy. 27.7 % of the curves were rejected overall.

*Transmission electron microscopy (TEM)*

Fascial tissue biopsies were collected and immediately placed in a fixative solution of 2.5 % (v/v) Glutaraldehyde/4 % paraformaldehyde in 0.1 M PIPES buffer (pH 7.2). The samples were fixed overnight at 4 °C. The following day, samples were washed with 0.1 M PIPES buffer (pH 7.2) and post-fixed in 1 % (v/v) osmium tetroxide in water. Samples were then dehydrated through a graded ethanol series before infiltration with Spurr resin (TAAB) and polymerization at 60 °C for 24 hrs. Ultra-thin sections (80 nm) were cut using an ultramicrotome (UC 7, Leica Microsystems, Vienna), mounted on copper grids and post-stained with Uranyless stain and Reynolds lead citrate. Samples were examined using the JEOL JEM-1400Flash (JEOL, Japan) operated at 80 kV and fitted with a 2MP JEOL Matataki camera. A total of 5 control and 4 RD fascial samples were analysed by TEM.

*Live cell imaging*

Cells were seeded at a density of 20,000 cells into 8-well chamber slide (Cellvis) in FGM. After 24 hrs cells were labelled with SPYDNA555 (1:1000 dilution) (Spirochrome) to label the nucleus and BioTracker490 Green Cytoplasmic dye (1:1000 dilution) (Sigma-Aldrich) in FGM media. Dyes were added 1 hr before imaging on a Nikon Ti2 wide-field imaging microscope at x20 magnification for 72 hrs.

*Interleukin-6 (IL-6) treatment assay*

FDFs were seeded onto 8-well chamber slides (Cellvis) in FGM. 24 hrs after seeding the wells were treated with 10 ng/ml of IL-6 in FGM and 0.25nmol/L AA. Control wells were cultured in FGM supplemented with 0.25 nmol/L AA. Cell cultures were decellularised [30], fixed with 4 % PFA and immunohistochemistry stained following previous immunohistochemistry methods described. CDMs were derived following the decellularisation method described above.

## Acknowledgements

We thank members of the clinical team at Great Ormond Street Hospital, Nicky Jessop, Caterine Miller, Gaynor Osman. We thank Eilleen Gentleman and the London Centre for Nanotechnology (LCN, London-nano.com), particularly Guillanne Charras, for their guidance in training and application of atomic force microscopy, Centre for Ultra-structural Imaging (CUI) at King's College London for processing tissue samples and use of electron microscopy equipment and the Nikon Imaging Centre (NIC), KCL for confocal microscopy. This work was funded by Medical Research Council (MRC) project grant, MRX000044_1.

## Supplementary materials

Supplementary material associated with this article can be found, in the online version, at doi:10.1016/j.matbio.2026.02.004.

## Data availability

Data will be made available on request.

## References

[1] A. Naba, Mechanisms of assembly and remodelling of the extracellular matrix, Nat. Rev. Mol. Cell Biol. 25 (11) (2024) 865–885.
[2] Z. Lansky, et al., 3D mapping of native extracellular matrix reveals cellular responses to the microenvironment, J. Struct. Biol. X 1 (2019) 100002.
[3] M.V. Plikus, et al., Fibroblasts: origins, definitions, and functions in health and disease, Cell 184 (15) (2021) 3852–3872.
[4] X. Huang, et al., Matrix stiffness-induced myofibroblast differentiation is mediated by intrinsic mechanotransduction, Am. J. Respir. Cell Mol. Biol. 47 (3) (2012) 340–348.
[5] L. Muhl, et al., Publisher correction: single-cell analysis uncovers fibroblast heterogeneity and criteria for fibroblast and mural cell identification and discrimination, Nat. Commun. 11 (1) (2020) 4493.
[6] M.B. Buechler, W. Fu, S.J. Turley, Fibroblast-macrophage reciprocal interactions in health, fibrosis, and cancer, Immunity 54 (5) (2021) 903–915.
[7] M. Torregrossa, et al., Effects of embryonic origin, tissue cues and pathological signals on fibroblast diversity in humans, Nat. Cell Biol. (2025).
[8] J.B. Parker, et al., Understanding fibroblast heterogeneity in form and function, Biomedicines (8) (2023) 11.
[9] J. Barallobre-Barreiro, et al., A sequential extraction methodology for cardiac extracellular matrix prior to proteomics analysis, Methods Mol. Biol. 1005 (2013) 215–223.
[10] J. Barallobre-Barreiro, et al., Cartilage-like composition of keloid scar extracellular matrix suggests fibroblast mis-differentiation in disease, Matrix. Biol. Plus. 4 (2019) 100016.
[11] M. Alexanian, et al., A transcriptional switch governs fibroblast activation in heart disease, Nature 595 (7867) (2021) 438–443.
[12] K. Theofilatos, et al., Proteomic Atlas of atherosclerosis: the contribution of proteoglycans to sex differences, plaque phenotypes, and outcomes, Circ. Res. 133 (7) (2023) 542–558.
[13] D.S. Foster, et al., Integrated spatial multiomics reveals fibroblast fate during tissue repair, Proc. Natl. Acad. Sci. U S. A (41) (2021) 118.
[14] K.Y. Deleon, et al., Extracellular matrix proteomics in cardiac ischemia/reperfusion: the search is on, Circulation 125 (6) (2012) 746–748.
[15] L. Cords, et al., Cancer-associated fibroblast classification in single-cell and spatial proteomics data, Nat. Commun. 14 (1) (2023) 4294.
[16] G. Biffi, D.A. Tuveson, Diversity and biology of cancer-associated fibroblasts, Physiol. Rev. 101 (1) (2021) 147–176.
[17] F. Zhang, et al., Defining inflammatory cell states in rheumatoid arthritis joint synovial tissues by integrating single-cell transcriptomics and mass cytometry, Nat. Immunol. 20 (7) (2019) 928–942.
[18] A.P. Croft, et al., Distinct fibroblast subsets drive inflammation and damage in arthritis, Nature 570 (7760) (2019) 246–251.
[19] S. Davidson, et al., Fibroblasts as immune regulators in infection, inflammation and cancer, Nat. Rev. Immunol. 21 (11) (2021) 704–717.
[20] P.P. Purslow, The structure and role of intramuscular connective tissue in muscle function, Front. Physiol. 11 (2020) 495.
[21] P.P.a.D.V.C. Purslow, Structure and function of intramuscular connective tissue, Connect. Tissue Matrix (1990) 127–166.
[22] M. Gumpenberger, et al., Remodeling the skeletal muscle extracellular matrix in older age-effects of acute exercise stimuli on gene expression, Int. J. Mol. Sci. (19) (2020) 21.
[23] V. Kovanen, Intramuscular extracellular matrix: complex environment of muscle cells, Exerc. Sport Sci. Rev. 30 (1) (2002) 20–25.
[24] N. Light, A.E. Champion, Characterization of muscle epimysium, perimysium and endomysium collagens, Biochem. J. 219 (3) (1984) 1017–1026.
[25] Y. Leng, et al., Extracellular matrix deposition precedes muscle-tendon integration during murine forelimb morphogenesis, Commun. Biol. 8 (1) (2025) 1202.
[26] P. Hasson, et al., Tbx4 and tbx5 acting in connective tissue are required for limb muscle and tendon patterning, Dev. Cell 18 (1) (2010) 148–156.
[27] L. Besse, et al., Individual limb muscle bundles are formed through progressive steps orchestrated by adjacent connective tissue cells during primary myogenesis, Cell Rep. 30 (10) (2020) 3552–3565, e6.

[28] G. Kardon, B.D. Harfe, C.J. Tabin, A Tcf4-positive mesodermal population provides a prepattern for vertebrate limb muscle patterning, Dev. Cell 5 (6) (2003) 937–944.
[29] M.A. Karsdal, et al., Extracellular matrix remodeling: the common denominator in connective tissue diseases. Possibilities for evaluation and current understanding of the matrix as more than a passive architecture, but a key player in tissue failure, Assay. Drug Dev. Technol. 11 (2) (2013) 70–92.
[30] G.R.F. Murphy, et al., Investigating the role connective tissue fibroblasts play in the altered muscle anatomy associated with the limb abnormality, Radial dysplasia, J. Anat. (2024).
[31] G.R.F. Murphy, et al., RADIATE - Radial Dysplasia Assessment, Treatment and Aetiology: protocol for the development of a core outcome set using a Delphi survey, Trials 20 (1) (2019) 339.
[32] C.A. van Nieuwenhoven, M. Mann, W. Hulsemann, The unsolved problem of radial longitudinal dysplasia: how can we reliably prevent recurrence, preserve growth and optimize function? J. Hand. Surg. Eur. Vol. 48 (3) (2023) 222–229.
[33] X. Shao, et al., MatrisomeDB 2.0: 2023 updates to the ECM-protein knowledge database, Nucleic. Acids. Res. 51 (D1) (2023) D1519–D1530.
[34] H. Kuivaniemi, G. Tromp, Type III collagen (COL3A1): gene and protein structure, tissue distribution, and associated diseases, Gene 707 (2019) 151–171.
[35] M. Asgari, et al., In vitro fibrillogenesis of tropocollagen type III in collagen type I affects its relative fibrillar topology and mechanics, Sci. Rep. 7 (1) (2017) 1392.
[36] R.J. Wenstrup, et al., Type V collagen controls the initiation of collagen fibril assembly, J. Biol. Chem. 279 (51) (2004) 53331–53337.
[37] K. Michalickova, et al., Mutations of the alpha2(V) chain of type V collagen impair matrix assembly and produce ehlers-danlos syndrome type I, Hum. Mol. Genet. 7 (2) (1998) 249–255.
[38] C. Moali, et al., Substrate-specific modulation of a multisubstrate proteinase. C-terminal processing of fibrillar procollagens is the only BMP-1-dependent activity to be enhanced by PCPE-1, J. Biol. Chem. 280 (25) (2005) 24188–24194.
[39] E.G. Tzortzaki, et al., Active remodeling in idiopathic interstitial pneumonias: evaluation of collagen types XII and XIV, J. Histochem. Cytochem. 54 (6) (2006) 693–700.
[40] S. Vadon-Le Goff, et al., Identification of PCPE-2 as the endogenous specific inhibitor of human BMP-1/tolloid-like proteinases, Nat. Commun. 14 (1) (2023) 8020.
[41] I.A. Omeis, Y.C. Hsu, M.S. Perin, Mouse and human neuronal pentraxin 1 (NPTX1): conservation, genomic structure, and chromosomal localization, Genomics 36 (3) (1996) 543–545.
[42] O. Rozenblatt-Rosen, et al., The Human Cell Atlas: from vision to reality, Nature 550 (7677) (2017) 451–453.
[43] B. Zhang, et al., A human embryonic limb cell atlas resolved in space and time, Nature (2023).
[44] K. De Filippo, et al., Mast cell and macrophage chemokines CXCL1/CXCL2 control the early stage of neutrophil recruitment during tissue inflammation, Blood 121 (24) (2013) 4930–4937.
[45] H. Mi, et al., Large-scale gene function analysis with the PANTHER classification system, Nat. Protoc. 8 (8) (2013) 1551–1566.
[46] H. Wang, et al., Tissue inhibitor of metalloproteinase 1 (TIMP-1) deficiency exacerbates carbon tetrachloride-induced liver injury and fibrosis in mice: involvement of hepatocyte STAT3 in TIMP-1 production, Cell Biosci. 1 (1) (2011) 14.
[47] B. Schoeps, J. Fradrich, A. Kruger, Cut loose TIMP-1: an emerging cytokine in inflammation, Trends. Cell Biol. 33 (5) (2023) 413–426.
[48] M.L. Iruela-Arispe, P. Hasselaar, H. Sage, Differential expression of extracellular proteins is correlated with angiogenesis in vitro, Lab. Invest. 64 (2) (1991) 174–186.
[49] M.L. Iruela-Arispe, E.H. Sage, Expression of type VIII collagen during morphogenesis of the chicken and mouse heart, Dev. Biol. 144 (1) (1991) 107–118.
[50] R. Kapoor, et al., Type VIII collagen has a restricted distribution in specialized extracellular matrices, J. Cell Biol. 107 (2) (1988) 721–730.
[51] N. Yamaguchi, et al., The cloning and sequencing of alpha 1(VIII) collagen cDNAs demonstrate that type VIII collagen is a short chain collagen and contains triple-helical and carboxyl-terminal non-triple-helical domains similar to those of type X collagen, J. Biol. Chem. 264 (27) (1989) 16022–16029.
[52] M. Sutmuller, J.A. Bruijn, E. de Heer, Collagen types VIII and X, two non-fibrillar, short-chain collagens. Structure homologies, functions and involvement in pathology, Histol. Histopathol. 12 (2) (1997) 557–566.
[53] A.L. Mohabeer, et al., Deletion of type VIII collagen reduces blood pressure, increases carotid artery functional distensibility and promotes elastin deposition, Matrix. Biol. Plus. 12 (2021) 100085.
[54] B.C. Hamel, et al., Ehlers-Danlos syndrome and type III collagen abnormalities: a variable clinical spectrum, Clin. Genet. 53 (6) (1998) 440–446.
[55] P.J. Haynes, et al., Atomic force microscopy of DNA and DNA-protein interactions, Methods Mol. Biol. 2476 (2022) 43–62.
[56] M.D.A. Norman, et al., Measuring the elastic modulus of soft culture surfaces and three-dimensional hydrogels using atomic force microscopy, Nat. Protoc. 16 (5) (2021) 2418–2449.
[57] A. Calo, et al., Spatial mapping of the collagen distribution in human and mouse tissues by force volume atomic force microsc, Sci. Rep. 10 (1) (2020) 15664.
[58] B. Hartmann, et al., Profiling native pulmonary basement membrane stiffness using atomic force microscopy, Nat. Protoc. 19 (5) (2024) 1498–1528.
[59] K.G. Danielson, et al., Targeted disruption of decorin leads to abnormal collagen fibril morphology and skin fragility, J. Cell Biol. 136 (3) (1997) 729–743.
[60] L.T. Smith, et al., Mutations in the COL3A1 gene result in the Ehlers-Danlos syndrome type IV and alterations in the size and distribution of the major collagen fibrils of the dermis, J. Invest. Dermatol. 108 (3) (1997) 241–247.
[61] A. Corsi, et al., Phenotypic effects of biglycan deficiency are linked to collagen fibril abnormalities, are synergized by decorin deficiency, and mimic Ehlers-Danlos-like changes in bone and other connective tissues, J. Bone Min. Res. 17 (7) (2002) 1180–1189.
[62] P. Bruckner, Suprastructures of extracellular matrices: paradigms of functions controlled by aggregates rather than molecules, Cell Tissue Res. 339 (1) (2010) 7–18.
[63] S.R. Pinnel, S. Murad, D. Darr, Induction of collagen synthesis by ascorbic acid. A possible mechanism, Arch. Dermatol. 123 (12) (1987) 1684–1686.
[64] S. Marcotti, et al., A workflow for rapid unbiased quantification of fibrillar feature alignment in biological images, Front. Comput. Sci. (2021) 3.
[65] G.R.F. Murphy, et al., Correction of "wrist" deformity in radial dysplasia: a systematic review and meta-analysis, J. Bone Jt. Surg. Am. 99 (24) (2017) 2120–2126.
[66] K.A. Robinson, et al., Decorin and biglycan are necessary for maintaining collagen fibril structure, fiber realignment, and mechanical properties of mature tendons, Matrix. Biol. 64 (2017) 81–93.
[67] S. Chakravarti, et al., Collagen fibril assembly during postnatal development and dysfunctional regulation in the lumican-deficient murine cornea, Dev. Dyn. 235 (9) (2006) 2493–2506.
[68] K.M. Meek, et al., An X-ray scattering investigation of corneal structure in keratocan-deficient mice, Matrix. Biol. 22 (6) (2003) 467–475.
[69] C. Bredrup, et al., Congenital stromal dystrophy of the cornea caused by a mutation in the decorin gene, Invest. Ophthalmol. Vis. Sci. 46 (2) (2005) 420–426.
[70] Y. Dong, J. Zhong, L. Dong, The role of decorin in autoimmune and inflammatory diseases, J. Immunol. Res. 2022 (2022) 1283383.
[71] C. Vuillermin, et al., Soft tissue release and bilobed flap for severe radial longitudinal deficiency, J. Hand. Surg. Am. 40 (5) (2015) 894–899.
[72] R. Harada, et al., Assessment of the upper limb muscles in patients with Fukuyama muscular dystrophy: noninvasive assessment using visual ultrasound muscle analysis and shear wave elastography, Neuromuscul. Disord. 32 (9) (2022) 754–762.
[73] P. Juhl, et al., IL-6 receptor inhibition modulates type III collagen and C-reactive protein degradation in rheumatoid arthritis patients with an inadequate response to anti-tumour necrosis factor therapy: analysis of connective tissue turnover in the tocilizumab RADIATE study, Clin. Exp. Rheumatol. 36 (4) (2018) 568–574.
[74] M.R. Duncan, B. Berman, Stimulation of collagen and glycosaminoglycan production in cultured human adult dermal fibroblasts by recombinant human interleukin 6, J. Invest. Dermatol. 97 (4) (1991) 686–692.
[75] Z.Q. Lin, et al., Essential involvement of IL-6 in the skin wound-healing process as evidenced by delayed wound healing in IL-6-deficient mice, J. Leukoc. Biol. 73 (6) (2003) 713–721.
[76] Y.H. Chen, et al., Inborn errors of IL-6 family cytokine responses, Curr. Opin. Immunol. 72 (2021) 135–145.
[77] B.K. Pedersen, M.A. Febbraio, Muscle as an endocrine organ: focus on muscle-derived interleukin-6, Physiol. Rev. 88 (4) (2008) 1379–1406.
[78] B.K. Pedersen, et al., Searching for the exercise factor: is IL-6 a candidate? J. Muscle Res. Cell Motil. 24 (2–3) (2003) 113–119.
[79] B.K. Pedersen, A. Steensberg, P. Schjerling, Muscle-derived interleukin-6: possible biological effects, J. Physiol. 536 (Pt 2) (2001) 329–337.
[80] F.N. Kenny, et al., Autocrine IL-6 drives cell and extracellular matrix anisotropy in scar fibroblasts, Matrix. Biol. 123 (2023) 1–16.